Phys Chem Minerals (2003) 30: 527–535
DOI 10.1007/s00269-003-0338-y

ORIGINAL PAPER

M. Tribaudino · F. Nestola · C. Meneghini
G. D. Bromiley

The high-temperature $P2/c_1$–$C2/c$ phase transition in Fe-free Ca-rich $P2_1/c$ clinopyroxenes

Received: 3 December 2002 / Accepted: 27 May 2003

Abstract An in situ, high-temperature, powder diffraction investigation was performed for iron-free clinopyroxenes with compositions $Ca_{0.40}Mg_{1.60}Si_2O_6$, $Ca_{0.52}Mg_{1.46}Al_{0.05}Si_{1.98}O_6$, $Ca_{0.59}Mg_{1.41}Si_2O_6$ and $Ca_{0.70}Mg_{1.30}Si_2O_6$, up to 850 °C using synchrotron radiation (ESRF, Grenoble). In samples with compositions $Ca_{0.52}Mg_{1.46}Al_{0.05}Si_{1.98}O_6$ and $Ca_{0.59}Mg_{1.41}Si_2O_6$, evidence of for the $P2_1/c$-$C2/c$ displacive phase transition was seen in changes in lattice parameters at $T \approx 550$ and 300 °C respectively. Landau modelling of the phase transition behaviour for the sample with composition $Ca_{0.52}Mg_{1.46}Al_{0.05}Si_{1.98}O_6$ shows a tricritical behaviour [$T_c = 547(16)$]. Comparison with the transition behaviour in other samples with lower Ca contents along the join diopside–enstatite indicates that a decrease in T_c, and a switch from first-order to tricritical behavior occurs with increasing Ca content. The change in the transition behaviour was related to an interaction with the antiphase domains at the nanoscale.

Keywords Clinopyroxene, In situ HT powder diffraction · Synchrotron radiation · Phase transition · Thermal expansion

M. Tribaudino (✉) · F. Nestola
Dipartimento di Scienze Mineralogiche e Petrologiche,
Università di Torino,
Via Valperga Caluso 35, 10125 Turin, Italy
e-mail: mario.tribaudino@unito.it
Tel: +39-011-6707131
Fax: +39-011-6707128

C. Meneghini
Dip. di Fisica E. Amaldi,
Università di Roma 3,
Via della Vasca Navale 84, 00146 Rome, Italy

G. D. Bromiley
Bayerisches Geoinstitut, Universität Bayreuth,
95440 Bayreuth, Germany

Introduction

Phase transitions in minerals have been the subject of numerous investigations, and provide important clues to understanding the thermal and compressional history of minerals, and in constraining the crystal-chemical behaviour with P and T. In pyroxenes, the most investigated phase transition is that from the $P2_1/c$ to $C2/c$ space group. In natural Ca-poor $P2_1/c$ pyroxenes, this transition occurs with increasing high pressure and temperature (Smyth and Burnham 1972; Angel et al. 1992). The $P2_1/c$-$C2/c$ high-pressure and high-temperature transition results in the formation of structurally different HT- and HP- $C2/c$ clinopyroxenes; tetrahedral chains are fully elongated in the HT-$C2/c$ structure, but they are highly kinked in the HP-$C2/c$ structure, and the oxygen packing is near that of cubic closed–packed structures (Angel et al. 1992; Angel and Hugh–Jones 1994; Hugh–Jones et al. 1994; Arlt et al. 1998; Ross and Reynard 1999; Arlt and Angel 2000).

Evidence for the occurence of the $P2_1/c$-$C2/c$ phase transition is given by the observation of antiphase domains, which have been widely observed in pigeonite from meteorite and volcanic rocks (Carpenter 1978, 1979; Mori and Takeda 1988; Pasqual et al. 2000), as well as in pyroxene-bearing rocks subjected to extreme pressure (Bozhilov et al. 1999). Antiphase domains can provide useful constraints to the cooling and decompressional history of a given pyroxene, once the stability of the $P2_1/c$ and $C2/c$ phases is determined as a function of pressure, temperature and composition.

Experimental work on the high-temperature $P2_1/c$ to $C2/c$ phase transition (Perrota and Stephenson 1965; Prewitt et al. 1971; Brown et al. 1972; Smyth and Burnham 1972; Smyth 1974; Sueno et al. 1984; Arlt et al. 2000) has shown that the transition temperature decreases from about 1000 to 200 °C as Ca and Fe increase from a hypothetical clinoenstatite end member. Single-crystal investigation on of clinoferrosilite (Smyth 1974) has shown that the transition is first-order. More

recently, this high-temperature transition has been reappraised, with new investigations aimed at modelling the thermodynamic behaviour using Landau theory (Camara et al. 2002; Tribaudino et al. 2002), and determining the precise effects of increasing Ca and Fe content, of exsolution-related microstructures and Fe–Mg cation order–disorder.

In natural pyroxenes, the effect of these variables may be difficult to distinguish. In contrast, for synthetic clinopyroxenes along the diopside–enstatite join (Di-En, $CaMgSi_2O_6$–$Mg_2Si_2O_6$), the effect of Ca for Mg substitution, and the related microtextures on the phase transition can be well constrained. Along this join, TEM analysis of diffraction patterns has shown that h + k odd reflections, indicative of a *P* lattice, are still present at room temperature in samples from 0 to 0.6 Ca atoms pfu (En–$Di_{60}En_{40}$, Tribaudino 2000). In clinoenstatite, and in a Ca-poor clinopyroxene with composition $Ca_{0.15}Mg_{1.85}Si_2O_6$, a first-order phase transition was observed with increasing temperature (Shimobayashi and Kitamura 1991; Shimobayashi et al. 2001; Tribaudino et al. 2002) and pressure (Angel et al. 1992; Nestola et al. 2002); and a decrease in transition temperature and pressure was noted with decreasing Ca content. In Ca-rich, intermediate clinopyroxene with the composition $Di_{50}En_{50}$, a high-pressure $P2_1/c$–$C2/c$ phase transition occurs (Tribaudino et al. 2001). However, an analysis of the spontaneous strain behaviour shows that the transition occurs with a smeared strain tail between 3 and 5 GPa, and deviates from first-order behaviour. In situ high-temperature single-crystal TEM observations were also performed for clinopyroxenes with compositions between $Di_{50}En_{50}$ and $Di_{60}En_{40}$. It was shown that critical h + k odd reflections are rather strong up to relatively high temperature; when the transition is eventually obtained, they become very diffuse, but are still present up to the highest achievable temperature (about 900 °C) even in grains with compositions very close to the transition (Tribaudino 2000). The dependence of critical temperature on composition and the thermodynamic character of the transition for these Ca-rich clinopyroxenes were not determined.

In this work, the results of a high-temperature in situ powder investigation up to $T = 850$ °C in three synthetic samples with composition $Ca_{0.4}Mg_{1.6}Si_2O_6$, $Ca_{0.52}Mg_{1.46}Al_{0.05}Si_{1.98}O_6$ and $Ca_{0.59}Mg_{1.41}Si_2O_6$ (hereafter $Di_{40}En_{60}$, $Di_{52}En_{46}CaTs_2$ and $Di_{60}En_{40}$, with CaTs Ca–Tschermak molecule, $CaAl_2SiO_6$) are reported. The aim of this study is to pinpoint the $P2_1/c$–$C2/c$ transition temperature and to determine the transition behaviour in $P2_1/c$ clinopyroxenes with intermediate Ca content along the join diopside–enstatite. For reference, the high-temperature cell evolution of a clinopyroxene with composition $Ca_{0.7}Mg_{1.3}Si_2O_6$ ($Di_{70}En_{30}$), and a constant $C2/c$ space group, has also been measured.

Experimental

Sample synthesis and characterization

The samples used in the high-temperature investigation were synthetized at high pressure, and at a temperature higher than that of the miscibility gap along the join diopside–enstatite (Gasparik 1990). The Al-free starting materials were gels of the nominal composition (mol%) $Di_{40}En_{60}$, $Di_{60}En_{40}$ and $Di_{70}En_{30}$. The $Di_{52}En_{46}CaTs_2$ clinopyroxene was obtained from a mixture of CaO, MgO, Al_2O_3 and SiO_2 oxides, with a composition calcualated on the basis of six oxygens of $Ca_{0.49}Mg_{1.29}Al_{0.11}Si_{2.03}O_6$. The oxide mixture and the gel $Di_{60}En_{40}$ were melted for 1 h at $T = 1600$ °C and room pressure to produce homogeneous melts, and quenched by plunging the crucible into water. The resulting glass was crushed and reground for 30 min in order to obtain a homogeneous mixture. Optical examination of the melted materials revealed complete vitrification. The gels with composition $Di_{40}En_{60}$ and $Di_{70}En_{30}$ were crystallized by annealing in an electrical furnace for 2 h at $T = 1380$ °C and 82 h at $T = 1350$ °C, respectively, to produce a crystalline starting material. The high-pressure syntheses were performed using a single-stage ½-inch piston cylinder with the hot-piston-in technique. A talc-pyrex cell has been used with a graphite furnace, tapered for the runs of the Al-bearing sample. Pressure was calibrated against the quartz–coesite and kyanite sillimanite transitions, as well as the melting point of diopside. Temperature was measured with a Pt–$Pt_{90}Rh_{10}$ thermocouple. No correction for the effect of pressure on thermocouple emf was applied. The experiment was quenched isobarically by shutting off the power whilst maintaining the pressure within 0.02 GPa of the run pressure. Quench rates are estimated to be greater than 100 °C s^{-1}. The synthesis conditions are reported in Table 1.

Samples were analyzed by X-ray powder diffraction (Guinier camera and CuK_α radiation), SEM-EDS analysis and transmission electron microscopy. The samples $Di_{60}En_{40}$ and $Di_{70}En_{30}$ were previously investigated by Tribaudino (2000).

TEM investigation was performed on a few grains of the synthesis products prepared by crushing in an agate mortar and subsequent deposition on a perforated carbon film. The TEM observations were made with a CM12 electron microscope operating at 120 kV and equipped with energy-dispersive spectrometer (EDS) analytical system and double tilt holder.

In all the experimental runs only clinopyroxene was crystallized. Al- and Si-enriched glass was observed in the Al-bearing sample.

Table 1 Annealing conditions, cell parameters and average cation EDS analyses (in atoms pfu) of the examined clinopyroxenes

	T (°C)	*P* (GPa)	*t* (h)	*a* (Å)	*b* (Å)	*c* (Å)	*β* (°)	*V* (Å^3)	Ca	Mg	Al	Si
[a]$Di_{70}En_{30}$	1500	18	2	9.720(2)	8.908(1)	5.243(1)	106.71(3)	434.9(2)	0.71	1.29	–	2.00
[a]$Di_{60}En_{40}$	1550	18	18	9.722(3)	8.900(2)	5.252(1)	107.22(3)	434.1(5)	0.59	1.42	–	2.00
$Di_{52}En_{46}CaTs_2$	1700	30	3.25	9.710(1)	8.887(1)	5.250(1)	107.37(1)	432.3(1)	0.52	1.46	0.05	2.00
$Di_{40}En_{60}$	1510	18	5	9.696(1)	8.875(1)	5.240(1)	108.10(1)	428.6(1)	0.40	1.60	–	2.00

[a] Tribaudino (2000)

In situ high-temperature synchrotron powder diffraction

The in situ high-temperature structural investigation was performed using synchrotron radiation powder diffraction. Synchrotron radiation allows highly resolved powder patterns to be obtained in a relatively short time. This was especially important for this work because samples have a tendency to exsolve quickly at T higher than 800 °C (Styrsa et al. 1999; Tribaudino et al. 2002), and exsolution-related microstructures have been found to significantly change the transition temperature (Tribaudino et al. 2002). The experiment was performed at ESRF (Grenoble, France), BM8 GILDA beamline, using an angle-dispersed setup based on a translating image plate camera, with fixed wavelength $\lambda = 0.61993$ Å (Meneghini et al. 2001). Sample powders were enclosed in quartz capillaries (inner diameter = 0.5 mm) and mounted horizontally on a goniometer head placed 300 mm from the translating image plate. The capillaries were kept rotating during the acquisition in order to improve the grain statistics. Samples were thermalized in the 100–800 °C range using a hot gas heater (Cyberstar). The image plate (IP) detector (200×400 mm^2) translates at constant speed behind a couple of vertical slits that select a thin portion of Debye–Sherrer diffraction rings. As motion is related with temperature increase, a continuous diffraction pattern as a function of time and temperature is recorded. The whole heating run lasts 2 h. The obtained 2-D images are processed by integrating vertical stripes at constant temperature. The heating system was calibrated against the quartz α–β phase transition. A small amount of Si standard was used as an internal calibrant (thermal expansion as in Keppler 1988) and was added to each of the examined samples and processed together with the pyroxene phase.

The diffraction patterns were quantitatively analyzed within the Rietveld structural refinement approach as implemented in the GSAS (Larson and Von Dreele 1986) package. The sample-to-image plate distance and instrumental line shape were calibrated from reference Si. A detailed description of the procedures followed in refining cell data can be found in Tribaudino et al. (2000). The obtained cell parameters are reported in Table 2. The error was obtained after applying a compression of the data up to conditions at which Durbin–Watson d statistics showed that no serial correlation was present (DWd, Hill and Flack 1987). This was done to avoid serial correlation related to diffraction pattern oversampling, that may lead to an underestimation of the experimental error (Hill 1992).

Results

TEM observations

Selected area electron diffraction patterns for samples $Di_{40}En_{60}$ and $Di_{52}En_{46}CaTs_2$ were taken to show h + k odd reflections indicative of a $P2_1/c$ symmetry. These reflections are very sharp for $Di_{40}En_{60}$, and have a slightly diffuse halo in $Di_{52}En_{46}CaTs_2$. In the sample $Di_{60}En_{40}$ $P2_1/c$ symmetry is present in most, but not all, crystals, and the h + k odd reflections are diffuse. In the sample $Di_{70}En_{30}$, h + k odd reflections were not found (Tribaudino 2000). Dark-field observations of h + k odd reflections confirm that the size of the antiphase domains decreases strongly with increasing Ca content. Along the join diopside–enstatite the domains are sized a few μm in $Di_{15}En_{85}$ (Tribaudino and Nestola 2002) and decrease from about 1 μm in $Di_{40}En_{60}$ (Fig. 1a) to 50–150 Å in $Di_{60}En_{40}$ (Fig. 4 in Tribaudino 2000). A mottled texture was present in grains with the composition $Di_{40}En_{60}$–$Di_{60}En_{40}$ (Fig. 1b), with an orientation almost parallel to (100) and (001). Mottled textures are not present in the clinopyroxene with composition $Ca_{0.15}Mg_{1.85}Si_2O_6$ (hereafter $Di_{15}En_{85}$) investigated by Tribaudino and Nestola (2002).

High-temperature powder diffraction

In Figs. 2 and 3 the evolution of the cell parameters for the studied samples is shown. Data for Ca-poor $Di_{15}En_{85}$ (Tribaudino et al. 2002), are also given for reference in Fig. 2. In $Di_{15}En_{85}$ the $P2_1/c$–$C2/c$ phase transition occurs at $T_{tr} = 991$ °C (Tribaudino et al. 2002), and the cell parameters undergo strong changes with temperature and a first-order step at the transition (Fig. 2). The $Di_{52}En_{46}CaTs_2$ and $Di_{60}En_{40}$ samples show a change in cell behaviour at approximately 550 and 300 °C, respectively, for the c and β cell parameters (Fig. 3). No significant change in slope is observed for the a and b parameters at these temperatures. The behaviour of the c and β parameters in $Di_{52}En_{46}CaTs_2$ and $Di_{60}En_{40}$ is similar to that of $Di_{15}En_{85}$ across the $P2_1/c$–$C2/c$ phase transition, implying that the same phase transition occurs in all samples. In samples $Di_{52}En_{46}CaTs_2$ and $Di_{60}En_{40,}$ the transition could be followed only by the cell-parameter evolution. The intensity of the critical h + k odd reflection, which were observed by TEM at room temperature in both samples, is too slight to be observed in the diffraction pattern.

The main difference in the phase transition for this work (Ca-rich) and Tribaudino et al. (2002) (Ca-poor $Di_{15}En_{85}$) is that the transition occurs with a continuous behaviour, compared with the markedly first-order transition observed in $Di_{15}En_{85}$. Similarly, at high pressure a similar change in the transition style for samples with different composition is is observed (Tribaudino et al. 2001; Nestola et al 2002).

In the sample $Di_{40}En_{60}$, the cell parameter evolution is like that observed in $P2_1/c$ in $Di_{15}En_{85}$ (Fig. 2), but up to 840 °C the transition is not achieved. In $Di_{40}En_{60}$, h + k odd reflections can be observed in the powder diffraction pattern. Their intensity decreases with increasing temperature (Fig. 4). At $T \geq 600$ °C, the h + k odd reflections become diffuse and hardly discernible form the background (Fig. 4); the only evidence for the $P2_1/c$ structure comes from the evolution with temperature of the cell parameters, that follows quite closely that of $Di_{15}En_{85}$. The critical reflections reappear during cooling at the same temperature.

Thermodynamic behaviour

The evolution of the order parameter (Q) with temperature was investigated in order to constrain the thermodynamic behaviour at the transition in $Di_{52}En_{46}CaTs_2$. Evolution of the order parameter can be obtained from the scalar spontaneous strain ε, that in this zone

Table 2 Cell parameters of the samples $Di_{40}En_{60}$, $Di_{52}En_{46}CaTs_2$, $Di_{60}En_{40}$ and $Di_{70}En_{30}$

T (°C)	a (Å)	b (Å)	c (Å)	β (°)	V (Å^3)
$Di_{40}En_{60}$					
150	9.715(2)	8.894(2)	5.248(1)	108.10(1)	431.1
187	9.718(2)	8.901(2)	5.250(1)	108.10(1)	431.7
246	9.724(2)	8.907(2)	5.253(1)	108.12(1)	432.4
317	9.729(2)	8.913(2)	5.256(1)	108.13(1)	433.1
382	9.734(2)	8.920(2)	5.259(1)	108.15(1)	433.9
435	9.740(2)	8.927(2)	5.261(1)	108.17(1)	434.6
475	9.745(2)	8.933(2)	5.264(1)	108.21(1)	435.3
521	9.751(2)	8.939(2)	5.268(1)	108.24(1)	436.1
571	9.758(2)	8.945(2)	5.272(1)	108.28(1)	436.9
612	9.765(2)	8.951(2)	5.275(1)	108.33(1)	437.7
663	9.772(2)	8.957(2)	5.280(1)	108.37(1)	438.6
706	9.779(2)	8.963(2)	5.284(1)	108.43(1)	439.4
746	9.787(2)	8.968(2)	5.289(1)	108.48(1)	440.3
793	9.795(2)	8.973(2)	5.294(1)	108.55(1)	441.1
844	9.803(2)	8.979(2)	5.298(1)	108.60(1)	442.0
858	9.807(2)	8.982(2)	5.301(1)	108.64(1)	442.4
$Di_{52}En_{46}CaTs_2$					
135	9.720(2)	8.890(2)	5.251(1)	107.50(1)	432.74
170	9.724(2)	8.894(2)	5.253(1)	107.52(1)	433.25
206	9.727(2)	8.898(2)	5.255(1)	107.53(1)	433.68
242	9.730(2)	8.902(2)	5.256(1)	107.55(1)	434.10
278	9.733(2)	8.906(2)	5.258(1)	107.57(1)	434.54
314	9.736(2)	8.911(2)	5.260(1)	107.58(1)	435.04
350	9.740(2)	8.914(2)	5.262(1)	107.59(1)	435.50
385	9.743(2)	8.919(2)	5.264(1)	107.61(1)	435.98
410	9.745(3)	8.923(3)	5.265(2)	107.60(2)	436.41
420	9.747(2)	8.924(2)	5.266(1)	107.62(1)	436.55
456	9.751(2)	8.928(2)	5.268(1)	107.64(1)	437.10
492	9.755(2)	8.934(2)	5.270(1)	107.68(1)	437.61
528	9.759(2)	8.938(2)	5.273(1)	107.72(1)	438.10
564	9.762(2)	8.943(2)	5.275(1)	107.74(1)	438.66
600	9.764(2)	8.946(2)	5.276(1)	107.77(1)	438.92
602	9.762(3)	8.945(3)	5.277(2)	107.76(2)	438.82
626	9.765(3)	8.949(3)	5.278(2)	107.77(2)	439.29
651	9.765(3)	8.952(3)	5.277(2)	107.82(2)	439.17
675	9.765(3)	8.953(3)	5.279(2)	107.85(2)	439.32
699	9.769(3)	8.958(3)	5.280(2)	107.83(2)	439.88
722	9.774(3)	8.959(3)	5.282(2)	107.82(2)	440.35
744	9.773(3)	8.963(3)	5.282(2)	107.84(2)	440.45
$Di_{60}En_{40}$					
100	9.730(1)	8.913(1)	5.2532(5)	107.31(1)	434.90
128	9.732(1)	8.914(1)	5.2546(5)	107.33(1)	435.25
157	9.734(1)	8.919(1)	5.2562(5)	107.34(1)	435.64
186	9.737(1)	8.922(1)	5.2575(6)	107.36(1)	435.98
213	9.739(1)	8.927(1)	5.2591(5)	107.37(1)	436.40
241	9.743(1)	8.930(1)	5.2617(6)	107.39(1)	436.86
270	9.745(1)	8.933(1)	5.2634(6)	107.42(1)	437.17
298	9.749(1)	8.936(1)	5.2658(5)	107.45(1)	437.63
327	9.750(1)	8.940(1)	5.2671(5)	107.46(1)	437.98
355	9.753(2)	8.944(2)	5.2691(6)	107.47(2)	438.45
384	9.757(1)	8.947(1)	5.2709(6)	107.49(1)	438.86
411	9.761(1)	8.950(1)	5.2722(6)	107.50(1)	439.27
440	9.763(1)	8.953(1)	5.2736(6)	107.51(1)	439.63
468	9.766(1)	8.956(1)	5.2752(6)	107.53(1)	439.99
496	9.769(1)	8.960(1)	5.2765(6)	107.54(1)	440.36
525	9.771(1)	8.963(1)	5.2780(6)	107.55(1)	440.75
553	9.774(1)	8.967(1)	5.2790(6)	107.56(1)	441.12
582	9.778(1)	8.970(1)	5.2806(6)	107.58(1)	441.51
611	9.781(1)	8.974(1)	5.2819(6)	107.59(1)	441.93
638	9.785(1)	8.977(1)	5.2835(6)	107.61(1)	442.34
666	9.786(1)	8.981(1)	5.2845(6)	107.61(1)	442.70
695	9.790(1)	8.984(1)	5.2854(6)	107.63(1)	443.02
723	9.792(1)	8.987(1)	5.2861(6)	107.64(1)	443.35
752	9.796(1)	8.991(1)	5.2879(6)	107.66(1)	443.79
781	9.798(1)	8.994(1)	5.2890(6)	107.66(1)	444.13

Table 2 (Contd.)

T (°C)	a (Å)	b (Å)	c (Å)	β (°)	V (Å^3)
$Di_{70}En_{30}$					
169	9.734(2)	8.931(2)	5.254(1)	106.82(1)	437.206
266	9.743(2)	8.941(2)	5.259(1)	106.89(1)	438.399
325	9.750(2)	8.949(2)	5.262(1)	106.92(1)	439.264
364	9.752(2)	8.954(2)	5.264(1)	106.95(1)	439.704
461	9.762(2)	8.966(2)	5.269(1)	107.00(1)	441.012
520	9.768(2)	8.974(2)	5.271(1)	107.04(1)	441.782
558	9.772(2)	8.980(2)	5.272(1)	107.05(1)	442.347
610	9.777(2)	8.988(2)	5.275(1)	107.07(1)	443.14
640	9.781(2)	8.992(2)	5.276(1)	107.09(1)	443.617
688	9.787(2)	9.001(2)	5.279(1)	107.10(1)	444.516
716	9.790(2)	9.005(2)	5.280(1)	107.11(1)	444.877
759	9.795(2)	9.014(2)	5.282(1)	107.13(1)	445.679

boundary transition couples with the Q as $\varepsilon \propto Q^2$. The spontaneous strain is calculated at each temperature from the low symmetry $P2_1/c$ cell parameters and those that the high temperature phase would have if extrapolated at the same temperature (Carpenter et al. 1998). A linear extrapolation for the high-T $C2/c$ cell parameters was performed; a linear fit proved suitable agreement with the experimental data also for $Di_{60}En_{40}$ ($C2/c$ at $T > 300$ °C) and $Di_{70}En_{30}$ which is always $C2/c$. The obtained thermal expansion coefficients are within the range observed for $C2/c$ pyroxenes, with $\alpha_b > \alpha_a > \alpha_c$ for all the investigated samples (Yang and Prewitt 2000; Table 3).

The spontaneous strain tensor for the transition has a major axis at about 20° from the c axis (160° from c measured from c to a). Such orientation is very close to that observed for the spontaneous strain in the high-temperature $P2_1/c$–$C2/c$ phase transition in $Di_{15}En_{85}$ (Tribaudino et al. 2002). Similarly, the other axes have a much smaller size; in $Di_{52}En_{46}CaTs_2$ they are not significant due to the small changes involved.

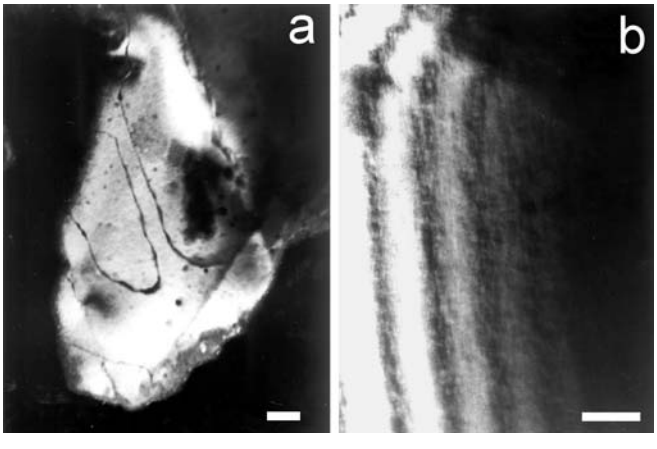

Fig. 1a Antiphase domains in sample $Di_{40}En_{60}$, view along [001]. Dark field, **g** = [210]; *bar* 0.1 μm. **b** Mottled texture in the same sample, view along [010]; dark field **g** = [402], *bar* 0.1 μm

In Fig. 5 the data for the ε_1 major strain axis are reported with temperature. As $\varepsilon_1 \propto Q^2$ the thermodynamic character for of the transition can be modelled by the standard Landau equation, as in $Di_{15}En_{85}$ (Tribaudino et al. 2002). The evolution of the macroscopic order parameter with temperature at equilibrium can be described via a polynomial expression as:

$$T = T_c - (b/a)Q^2 - (c/a)Q^4$$

A fit of the data in Fig. 5 gives for $Di_{52}En_{46}CaTs_2$:

$$T = 547(16) + 0.2(4)Q^2 - 0.015(3)Q^4$$

In the obtained fit, the quadratic term does not significantly deviate from 0, i.e. a tricritical behaviour is observed, with a $T_c = 547(16)$ °C. In $Di_{15}En_{85}$ a first-order behaviour is instead present, with a large step at the transition and a $T_c = 926(39)$ °C. The switch from a first order to a continuous-phase transition with composition was also observed for the high-pressure phase transition. In clinoenstatite and $Di_{15}En_{85}$, the transition is clearly first-order, with a step at the transition, whereas for $Di_{50}En_{50}$ the spontaneous strain undergoes a continuous decrease down to 5 GPa. At higher pressure the cell parameters follow the trend of HP-$C2/c$ (Tribaudino et al. 2001).

Discussion

The above results indicate that along the join diopside–enstatite a decrease in the T_c and a change in the transition behaviour with increasing Ca occur.

The decrease in the T_c is in agreement with previous findings (Prewitt et al. 1971; Arlt et al. 2000). The observed decrease is less than expectable for intermediate clinopyroxenes: the investigated samples are very close to

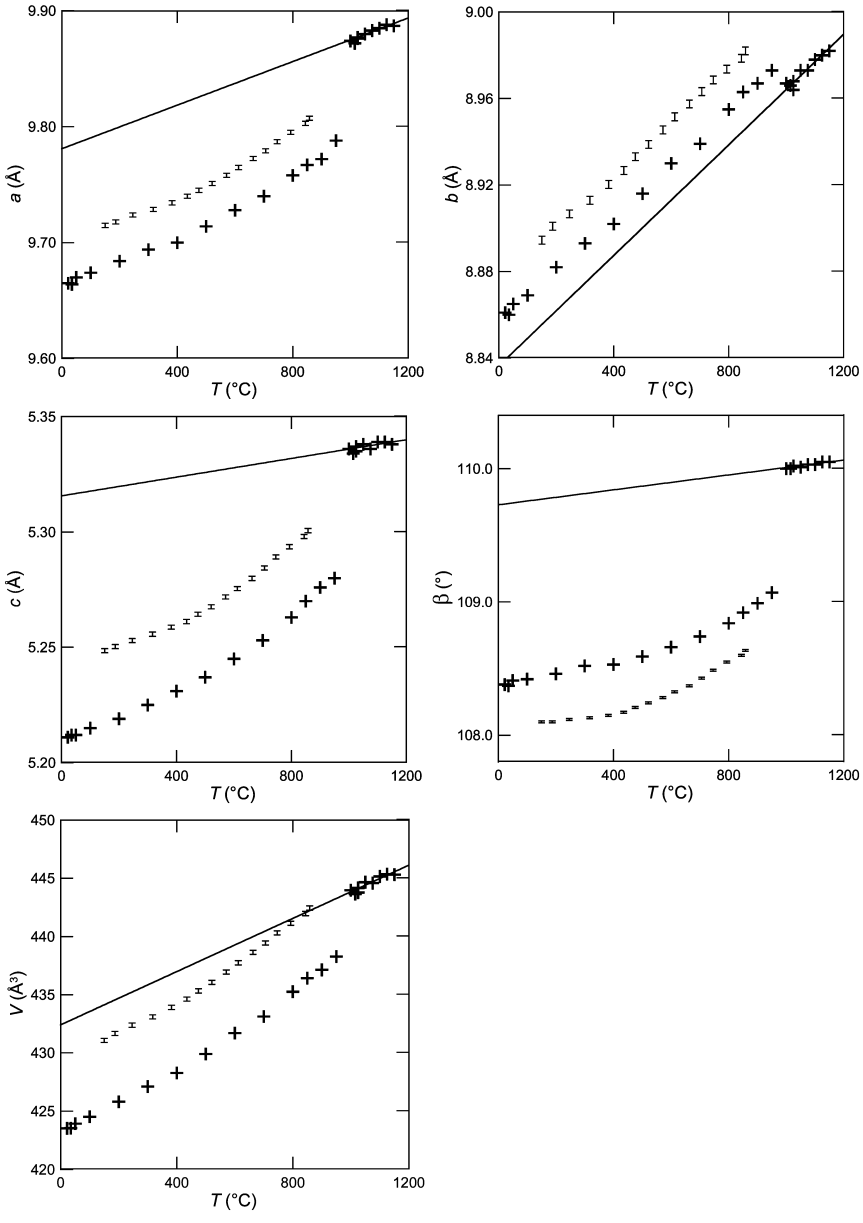

Fig. 2 Cell parameters with T in $Di_{15}En_{85}$ (*crosses* Tribaudino et al. 2002) and $Di_{40}En_{60}$ (*error bars* this work). The trend for the $C2/c$ structure in $Di_{15}En_{85}$ is shown

the transition at room T (at $Di_{60}En_{40}$; Tribaudino et al. 2002), yet their T_c is relatively high. For instance, Arlt et al. (2000), on the basis of the M2 average cation radius, would predict for the samples $Di_{52}En_{46}CaTs_2$ and $Di_{60}En_{40}$ a T_c of at most 300 and 100 °C, respectively. The presence of compositional modulations may account for the increase in T_c: in $Di_{15}En_{85}$ it was observed that compositional modulations stabilize the $P2_1/c$ phase, increasing its T_c. TEM evidence shows that modulations for compositions higher than $Di_{60}En_{40}$ vanish with increasing Ca content, and at $Di_{65}En_{35}$ no evidence of modulations can be observed (Tribaudino 2000).

The change in the thermodynamic behaviour of the transition can be related to increasing Ca content (as in Camara et al. 2002) and to Ca-related microstructures. Microstructures induce a strain that may interact with the spontaneous strain of the transition. Ca substitution induces the presence of mottled textures, preliminary to exsolution, and is related to a decrease in the size of the antiphase domains.

Mottled textures do not seem by themselves to induce a change in the transition order. In Ca-poor $Di_{15}En_{85}$, a first-order behaviour, albeit with different transition temperature, was observed in a crystal free of modulations and in the same crystal with modulations induced by prolonged heating. Landau modelling of the transition behaviour shows that in the modulated sample, the behaviour is even more first-order than in the unstrained sample, having a larger quadratic term (Tribaudino et al. 2002).

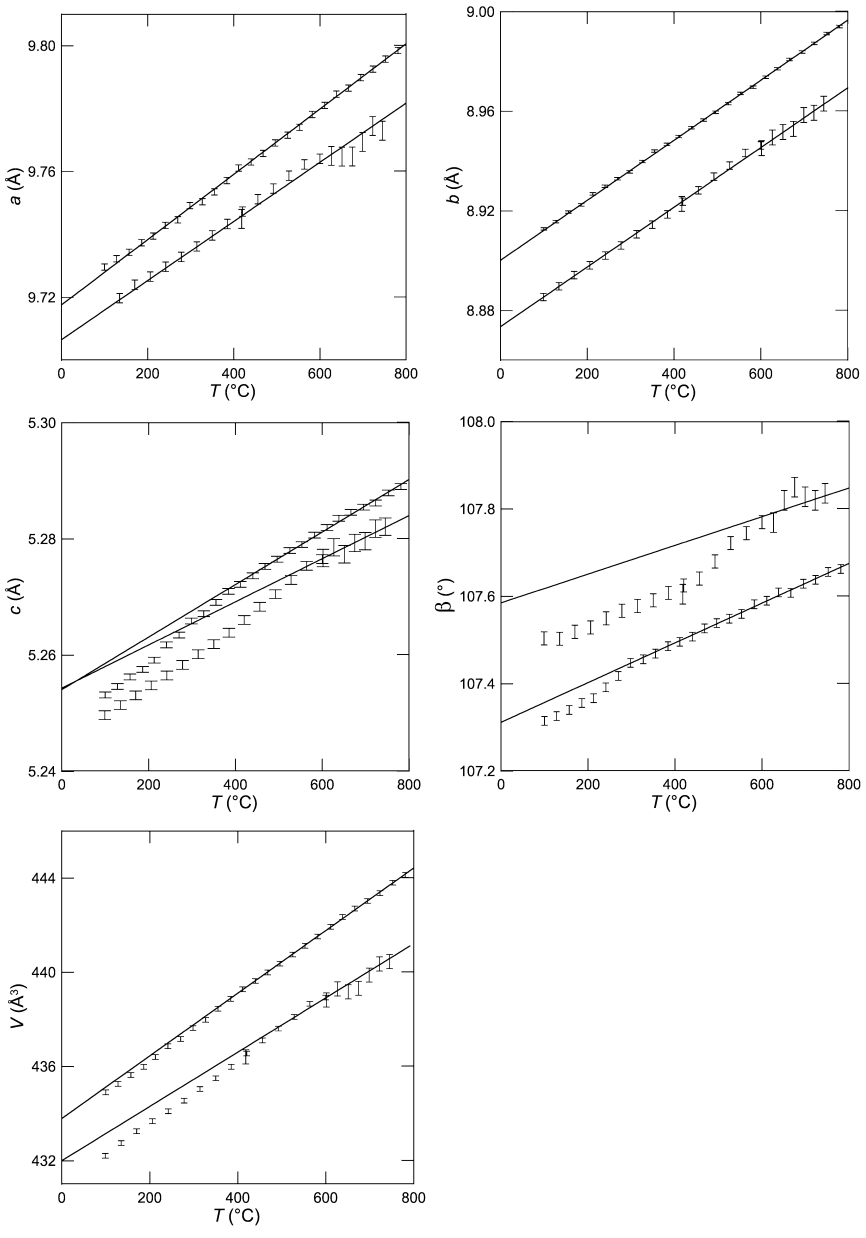

Fig. 3 Cell parameters with T in $Di_{52}En_{46}CaTs_2$ and $Di_{60}En_{40}$. The $Di_{52}En_{46}CaTs_2$ trend refers to the plot below in all but the β vs T plot

The size of the domains decreases dramatically from $Di_{40}En_{60}$ to $Di_{60}En_{40}$. This is probably related to the presence of Ca-rich clusters, with local $C2/c$ structure, due to compositional fluctuations. These clusters are clearly more common between $Di_{52}En_{46}CaTs_2$ and $Di_{60}En_{40}$. It was shown that the domains have $P2_1/c$ structure and are separated by $C2/c$ boundaries (Carpenter 1978). This was confirmed for samples along the join diopside–enstatite with composition $Di_{54}En_{46}$ by high-resolution TEM observation of Styrsa et al. (1999). The domains are limited by the presence of these clusters, which are pinned at the boundaries. As a result, the microstructure of $Di_{52}En_{46}CaTs_2$ and $Di_{60}En_{40}$ is made up by $P2_1/c$ nanodomains, separated by rather large boundaries. In sample $Di_{40}En_{60}$. compositional fluctuations and hence clusters with Ca content higher than the average are probably present, as indicated by the mottled texture. The composition of the clusters is probably Ca-poorer than in $Di_{52}En_{46}CaTs_2$, and they have a $P2_1/c$ local structure. Therefore they do not have a pinning effect on the antiphase domain size, that are is still very large (Fig. 1a).

For our samples, local strain arises at the boundaries for local Ca concentrations, that may couple with the $P2_1/c$–$C2/c$ phase transition. The higher boundary frequency in $Di_{52}En_{46}CaTs_2$ and $Di_{60}En_{40}$ induces an overall higher strain for these compositions. An evidence for a strain effect at the domains is the presence of a

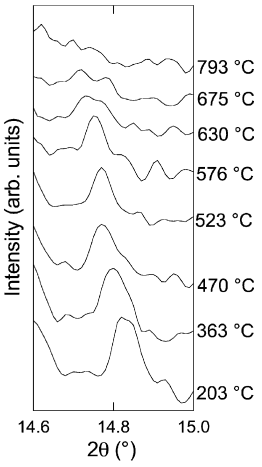

Fig. 4 The critical (23$\bar{1}$) reflection with temperature in $Di_{40}En_{60}$. The same reflection was found as evidence for the $P2_1/c$ structure in $Di_{30}En_{70}$ by Newton et al. (1979). Note *peak broadening* at $T > 600$°C

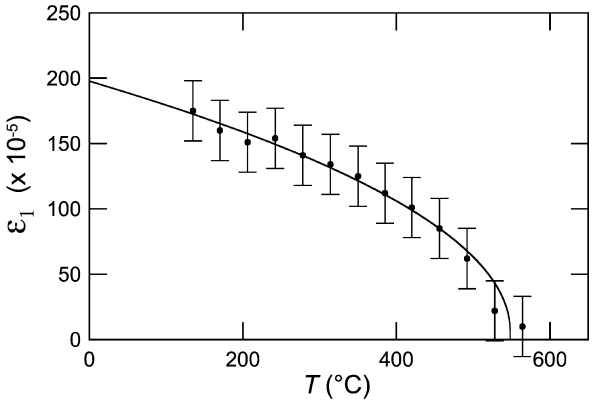

Fig. 5 Evolution with T of major axis of the spontaneous strain ellipsoid (at 160° from c, measured from c towards a) $\varepsilon_1 \propto Q^2$ for the $P2_1/c$–$C2/c$ phase transition. The trend obtained for the tricritical fit as discussed in the text is reported

preferential orientation in the antiphase domains of the sample $Di_{52}En_{46}CaTs_2$ and $Di_{60}En_{40}$ (Nord 1992; Tribaudino 2000). The presence of a non-first-order $P2_1/c$-$C2/c$ phase transitition was also observed in the natural Ca- and Fe-rich pigeonite BTS308 (Camara et al. 2002), in which antiphase domains comparable in size to those observed in $Di_{52}En_{46}CaTs_2$ and $Di_{60}En_{40}$ are present (Pasqual et al. 2000). In the BTS308 pigeonite however, other effects, like possible coupling with Fe–Mg order–disorder, have to be considered (Camara et al. 2002).

Some suggestion on the microscopic mechanism of the transition can also be proposed. In the sample $Di_{40}En_{60}$ the critical reflections almost disappear, before the actual achievement of the transition is documented by changes in cell parameters. The $Di_{40}En_{60}$ sample is indeed chemically heterogeneous, as shown by the presence of a mottled texture. However, in contrast to $Di_{52}En_{46}CaTs_2$ and $Di_{60}En_{40}$, the antiphase domains are very large, indicating that local inhomogeneities have $P2_1/c$ structure. Heating at high temperature would, however, promote the transition of Ca-richer clusters that reach their transition temperature. This would locally break the $P2_1/c$ structure, inducing the formation of small sized antiphase domains, and of diffuse h + k odd reflections. Data from the present study suggest that this may happen at approximately 600 °C in $Di_{40}En_{60}$ at which point the h + k odd reflections disappear from the powder pattern (Fig. 4). At higher temperatures, the $Di_{40}En_{60}$ probably displays the same structure observed at room T by Ca-richer samples $Di_{52}En_{46}CaTs_2$ and $Di_{60}En_{40}$. In $Di_{52}En_{46}CaTs_2$ and in $Di_{60}En_{40}$ small antiphase domains are already present at room T; h + k odd reflections are too faint to be revealed by powder diffraction, but can be observed with TEM. At higher temperatures, the domain boundaries are expected to increase up to a size at which the domains become uncorrelated and diffusion in critical reflections is observed with the TEM. Such diffusion is pinned by Ca-poor areas and persists even at high temperature, as documented by Tribaudino (2000) by in situ TEM investigation. A similar behaviour was observed with pressure for the sample with composition $Di_{50}En_{50}$ (Tribaudino et al. 2001). In this sample the h + k odd (23$\bar{1}$) reflection almost disappears at $P = 2.8$ GPa, but the cell parameters follow the trend for HP-$C2/c$ only at P > 5 GPa. The intensity of the h + k even reflection (131) increases between 2.8 and 5 GPa up to the value in the HP-$C2/c$. A further increase in pressure does not significantly change the intensity of the (131) reflection. This suggests that the amount of the $C2/c$ phase increases with pressure up to completion of the transition, most likely by an increase in the size of the domain boundaries.

The proposed mechanism of phase transition by growth of $C2/c$ domain boundaries is in agreement with high-temperature TEM observations by Shimobayashi and Kitamura (1991) of the evolution of the antiphase boundaries throughout the transition in Ca-poor lamellae of composition $Ca_{0.06}Mg_{1.16}Fe_{0.78}Si_2O_6$ of an exsolved pigeonite.

Table 3 Thermal expansion coefficients [for a given cell parameter cp: $\alpha_{cp} = (1/cp_0)\partial cp/\partial T$] of the $C2/c$ phase

	α_a	α_b	α_c	α_β	α_V
$Di_{15}En_{850}$	1.08(12)	1.34(15)	0.46(16)	3.0(5)	2.7(4)
$Di_{52}En_{46}CaTs_2$	0.92(16)	1.35(9)	0.72(11)	3.5(1.7)	2.8(4)
$Di_{60}En_{40}$	1.07(1)	1.35(6)	0.86(2)	4.24(8)	3.1(2)
$Di_{70}En_{30}$	1.06(2)	1.56(7)	0.89(1)	4.83(17)	3.27(11)

Acknowledgements This work was supported by CNR and MIUR grants (project: Structural evolution and phase transitions in minerals versus temperature, pressure and composition).

References

Angel RJ, Hugh Jones DA (1994) Equations of state and thermodynamic properties of enstatite pyroxenes. J Geophys Res 99: 19777–19783

Angel RJ, Chopelas A, Ross NL (1992) Stability of high-density clinoenstatite at upper mantle pressures. Nature 358: 322–324

Arlt T, Angel RJ (2000) Displacive phase transitions in C-centered clinopyroxenes: spodumene, $LiScSi_2O_6$ and $ZnSiO_3$. Phys Chem Miner 27: 719–731

Arlt T, Angel RJ, Miletich R, Armbruster T, Peters T (1998) High-pressure $P2_1/c$–$C2/c$ phase transitions in clinopyroxenes: influence of cation size and electronic structure. Am Mineral 83: 1176–1181

Arlt T, Kunz M, Stoltz J, Armbruster T, Angel RJ (2000) *P–T–X* data on $P2_1/c$ clinopyroxenes and their displacive phase transitions. Contrib Mineral Petrol 138: 35–45

Bozhilov KN, Green II HW, Dobrzhinetskaya L (1999) Clinoenstatite in Alpe Arami peridotite: additional evidence of very high pressure. Science 284: 128–132

Brown GE, Prewitt CT, Papike JJ, Sueno S (1972) A comparison of the structures of low and high pigeonite. J Geophys Res 77: 5778–5789

Cámara F, Carpenter MA, Domeneghetti MC, Tazzoli V (2002) Non-convergent ordering and displacive phase transition in pigeonite: in-situ HT XRD study. Phys Chem Miner 29: 331–340

Carpenter MA (1978) Nucleation of augite at antiphase boundaries in pigeonite. Phys Chem Miner 2: 237–251

Carpenter MA (1979) Experimental coarsening of antiphase domains in a silicate mineral. Science 206: 681–683

Carpenter MA, Salje EKH, Graeme-Barber A (1998) Spontaneous strain as a determinant of thermodynamic properties for phase transition in minerals. Eur J Mineral 10: 621–691

Gasparik T (1990) A thermodynamic model for the enstatite–diopside join. Am Mineral 75:1080–1091

Hill RJ (1992) Rietveld refinement round robin. I. Analysis of standard X-ray and neutron data for $PbSO_4$. J Appl Crystallogr 25: 589–610

Hill RJ, Flack HD (1987) The use of Durbin Watson d statistics in Rietveld analysis. J Appl Crystallogr 20: 356–361

Hugh-Jones DA, Woodland AB, Angel RJ (1994) The structure of high pressure $C2/c$ ferrosilite and crystal chemistry of high-pressure $C2/c$ pyroxenes. Am Mineral 79: 1032–1041

Keppler U (1988) Thermal expansion of silicon. Z Metallkunde 79: 157–158

Larson AC, Von Dreele RB (1986) GSAS: General software analysis system manual. Los Alamos National Laboratory Report. LA-UR:86–87

Meneghini C, Artioli G, Balerna A, Gualtieri AF, Norby P, Mobilio S (2001) A translating imaging plate system for in-situ experiments at the GILDA beamline. J Synchr Rad 8: 1162–1166

Mori H, Takeda H (1988) Stress induced transformation of pigeonites from achondritic meteoritics. Phys Chem Miner 15: 252–259

Nestola F, Tribaudino M, Boffa Ballaran T (2002) The high-pressure $P2_1/c$ – $C2/c$ phase transition for the CMS (CaO – MgO – SiO_2) clinopyroxene. J Conf Abstracts 7: 79

Nord GL (1992) Imaging transformation induced microstructures. In: Buseck PR (ed) Minerals and reactions at the atomic scale: transmission electron microscopy. Reviews in Mineralogy vol 27: 455–508 Mineralogical Society of America Washington DC

Pasqual D, Molin G, Tribaudino M (2000) Single-crystal thermometric calibration of Fe–Mg order–disorder in pigeonites. Am Mineral 85: 953–962

Perrota AJ, Stephenson DA (1965) Clinoenstatite: high-low inversion. Science 148: 1090–1091

Prewitt CT, Brown GE, Papike JJ (1971) Apollo 12 clinopyroxenes. High-temperature X-ray diffraction studies. Geoch Cosmoch Acta 1; Suppl 2: 59–68

Ross NL, Reynard B (1999) The effect of iron on the $P2_1/c$ to $C2/c$ transition in $(Mg,Fe)SiO_3$ clinopyroxenes. Eur J Mineral 11: 585–589

Shimobayashi N, Kitamura M (1991) Phase transition in Ca-poor clinopyroxenes: a high-temperature transmission electron microscopic study. Phys Chem Miner 18: 153–160

Shimobayashi N, Miyake A, Kitamura M, Miura E (2001) Molecular dynamics simulations of the phase transition between low-temperature and high-temperature clinoenstatites. Phys Chem Miner 28: 591–599

Smyth JR (1974) The high-temperature crystal chemistry of clinohypersthene. Am Mineral 59: 1061–1082

Smyth JR, Burnham CW (1972) The crystal structures of high and low clinohypersthene. Earth Planet Sci Lett 14: 183–189

Styrsa VJ, Weinbruch S, Muller WF (1999) A transmission electron microscopy study of exsolution and coarsening in iron-free clinopyroxene. Lunar Planet Sci 30: #1111

Sueno S, Kimata M, Prewitt CW (1984) The crystal structure of high clinoferrosilite. Am Mineral 69: 265–269

Tribaudino M (2000) A transmission electron microscope investigation on the $C2/c$ –$P2_1/c$ phase transition in clinopyroxenes along the diopside-enstatite ($CaMgSi_2O_6$–$Mg_2Si_2O_6$) join. Am Mineral 85: 707–715

Tribaudino M, Nestola F (2002) Average and local structure in $P2_1/c$ clinopyroxenes along the join diopside–enstatite ($CaMgSi_2O_6$–$Mg_2Si_2O_6$). Eur J Mineral 14: 549–555

Tribaudino M, Prencipe M, Bruno M, Levy D (2000) High pressure behaviour of Ca-rich $C2/c$ clinopyroxenes along the join diopside-enstatite ($CaMgSi_2O_6$ $Mg_2Si_2O_6$). Phys Chem Miner 27: 656–664

Tribaudino M, Prencipe M, Nestola F, Hanfland M (2001) A $P2_1/c$–$C2/c$ high-pressure phase transition in $Ca_{0.5}Mg_{1.5}Si_2O_6$ clinopyroxene. Am Mineral 86: 807–813

Tribaudino M, Nestola F, Cámara F, Domeneghetti MC (2002) The high-temperature $P2_1/c$–$C2/c$ phase transition in Fe-free pyroxenes: structural and thermodynamic behavior. Am Mineral 87: 648–657

Yang H, Prewitt CT (2000) Chain and layer silicates at high temperatures and pressures. In: Hazen RM, Downs RT (eds) High-temperature and high-pressure crystal chemistry. Rev Mineral Geochem 41: 211–255